Eur. Phys. J. D **44**, 313–317 (2007)
DOI: 10.1140/epjd/e2007-00193-6

THE EUROPEAN PHYSICAL JOURNAL D

Experimental measurements of K X-ray production cross-sections and yields for the elements with $58 \leqslant Z \leqslant 64$ at 123.6 keV photon energy

B. Ertuğral[a]

Department of Physics, Faculty of Art and Sciences, Giresun University, 28000 Giresun, Turkey

Received 18 September 2006 / Received in final form 22 November 2006
Published online 13 June 2007

Abstract. Considering the importance of the K X-ray production cross-sections ($\sigma^{x}_{K_i}$) as well as the K shell fluorescence yields (ω_K) for the determination of element concentrations in a given material, we have measured them experimentally for the elements Ce, Pr, Nd, Sm, Eu and Gd using photons at 123.6 keV from a ^{57}Co radioisotope source. Furthermore, the K X-rays intensity ratios (K_β/K_α) for these elements have been investigated. The characteristic K X-rays emitted by the target were detected by a high-resolution with an energy resolution of 160 eV full with at half-maximum ($FWHM$) at 5.96 keV. The experimental results of K X-ray production cross-sections were compared with theoretically predicted values based on relativistic Hartree-Slater and Hartree-Fock theories. Similarly, the measured K shell fluorescence yields/cross-sections and the K X-rays intensity ratios were compared with the theoretical values. In most cases, there is an agreement between the experimental and theoretical data within the experimental uncertainties.

PACS. 32.30.Rj X-ray spectra – 32.80.Cy Atomic scattering, cross-sections, and form factors; Compton scattering – 32.80.-t Photon interactions with atoms – 30.70.-n Intensities and shapes of atomic spectral lines

1 Introduction

X-ray emission is a phenomenon resulting from the decay of atoms after bombardment by charged particles or electromagnetic radiation. The study of this phenomenon is very important for atomic, molecular and radiation physics investigations, material analysis especially in medical, geological and environmental fields using energy-dispersive X-ray fluorescence (EDXRF) [1].

In recent decades, considerable efforts have been directed to the study of X-ray fluorescence (XRF) yields, K_β/K_α intensity ratios and K X-ray production cross-sections. As a result of this effort, Rao et al. [2] and Al-Nasr et al. [3] have measured K-shell fluorescence cross-sections and yields using radioisotope and X-ray tubes. The K_α and K_β X-ray fluorescence cross-sections for some elements with $73 \leqslant Z \leqslant 82$ have been studied by Saleh and Al-Saleh [4]. Ertuğrul [5] measured K, L and higher shell photoionization cross-sections using ^{241}Am radioisotope source (59.5 keV γ-rays) and Si(Li) detector. Some researchers theoretically calculated K and L X-ray fluorescence cross-sections [6].

K shell fluorescence yields ω_K were deduced from the measured cross-sections by using the theoretical photoionization cross-sections and fractional X-ray emission rates. Bambynek et al. [7] in a review article have fitted their collection of selected most reliable experimental values in the $13 \leqslant Z \leqslant 92$ range. Krause [8] compiled ω_K adopted values for elements $5 \leqslant Z \leqslant 110$. Hubbell et al. [9] have compiled more recent experimental values.

K shell X-ray intensity ratios (K_β/K_α) for elements, compounds and complexes have been investigated (theoretically and experimentally) by various authors (Ertuğrul et al. [10], Dhal and Padhi [11], Ertuğrul and Şimşek [12], Rao et al. [13], Çevik et al. [14], Scofield [15,16].

There are several studies concerning with K X-ray production cross-sections in the literature using the ^{57}Co radioisotope. Saleh and El-Haija [17] and Seven [18] measured photon-induced K X-ray cross-sections for some heavy elements. Apaydin and Tirasoğlu [19] have measured K shell X-ray production cross-sections and fluorescence yields of elements in the atomic number range $65 \leqslant Z \leqslant 92$. Bennal et al. [20] measured K X-ray fluorescence parameters for Ag, Cd, In and Sn elements. In addition, Özdemir et al. [21] measured K shell X-ray production cross-sections for Cd, In, Sb, Te, I, Ba, La, Ce, Nd, Sm, Tb and Dy 59.54 keV γ-rays from an ^{241}Am radioisotope source. Durak et al. [22] experimentally determined K_i ($i = \alpha$ and β) X-ray cross-sections for K_α and K_β X-ray line for Zr, Mo, Ag, In, Sn, Ba, Ce, Nd, Gd, Dy, Er and Yb elements using 122 keV photons.

[a] e-mail: ertugral@ktu.edu.tr

In the present investigation, we have measured the K X-ray production cross-sections, K shell fluorescence yields and K X-ray intensity ratios (K_β/K_α) of 6 elements in the atomic range $58 \leqslant Z \leqslant 64$ (Ce, Pr, Nd, Sm, Eu and Gd). The targets were ionized using 123.6 keV photons from a ^{57}Co radioisotope source, and the emitted K X-rays and scattered γ-rays were detected using a Si(Li) detector. The results of K X-ray production cross-sections were then compared with the corresponding calculated theoretical values based on relativistic Hartree-Fock and Hartree-Slater theories. To best of our knowledge, K_i ($i = \alpha_1$, α_2, β_1 and β_2) X-ray production cross-sections for these elements (Ce, Pr, Nd, Sm, Eu and Gd) at this energy are being reported for the first time.

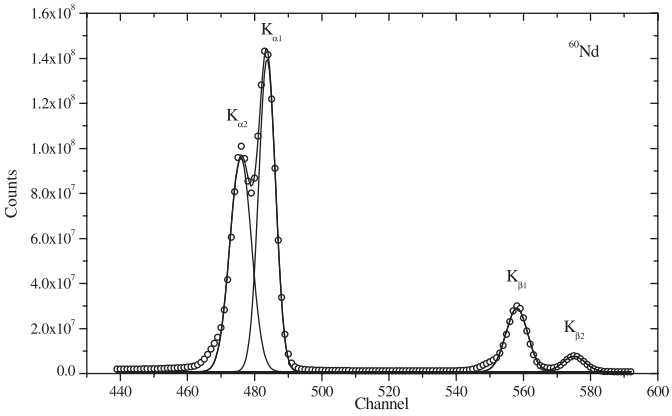

Fig. 1. Typical K X-ray spectrum for Nd irradiated with 123.6 keV gamma rays emitted from ^{57}Co.

2 Experimental details

The geometry and the shielding arrangements of the experimental set-up employed in the present work have been described elsewhere [23]. The samples were irradiated with a ^{57}Co radioisotope source emitting 123.6 keV photons with strength of approximately 25 mCi. The radioactive source ^{57}Co decays by electron conversion process into metastable states of ^{57}Fe and in turn it γ-photons of energies 122 (85%), 136 (11%) and 14.4 (8.5%). Since the intensity of the 122 keV photons is predominant over that of the 136 keV photons and as they are close to each other, we can take the weighted average of 122 keV and 136 keV, i.e. 123.6 keV. Spectroscopically, high purity (99.90%) targets of CeO_2, Pr_3O_4, Nd_2O_3, Sm_2O_3, Eu_2O_3 and Gd_2O_3 of thickness ranging from 20 to 40 mg/cm^2 have been used for the measurements. The samples were then placed at 45° angle with respect to the direct beam and fluorescent X-rays emitted 90° to the detector. The incident beam and fluorescence X-rays emitted from the target were detected with a Si(Li) detector manufactured by Canberra ($FWHM = 160$ eV at 5.9 keV, active area 13 mm^2, thickness 3 mm and Be window thickness 30 μm). The output from the preamplifier, with pulse pile-up rejection capability, was fed to a multi-channel analyzer interfaced with a personal computer provided with suitable software (Tennelec PCA II) for data acquisition and peak analysis. The lifetime was selected to be 5000 s for all elements. Figure 1 shows a typical K X-ray spectrum for Nd.

3 Data analysis

3.1 Experimental method

The experimental K X-ray production cross-sections $\sigma^{\mathrm{x}}_{K_i}$(cm^2/g) were obtained from the equation [24]

$$\sigma^{\mathrm{x}}_{K_i} = \frac{N_{K_i}}{I_0 G \varepsilon_{K_i} \beta_{K_i} m} \tag{1}$$

where N_{K_i} ($i = \alpha_1$, α_2, β_1, β_2) is the net counts per unit time under the associated elemental photopeak; I_0G, the intensity of exciting radiation falling on sample; ε_{K_i}, the detector efficiency for the K X-rays of the element; m is the mass thickness of target in g cm^{-2} and β_{K_i} the self-absorption given by

$$\beta = \frac{1 - \exp\left[-\left(\mu_{inc}/\sin\theta + \mu_{emt}/\sin\phi\right) t\right]}{\left(\mu_{inc}/\sin\theta + \mu_{emt}/\sin\phi\right) t} \tag{2}$$

where μ_{inc} and μ_{emt} are the total mass absorption coefficients (from XCOM is database program in the electronic version [25]) of target material at the incident photon energy and at the emitted average K_α and K_β X-ray energies [26] and t is the thickness of the target in g cm^{-2}, θ and ϕ are the angles of incident photon and emitted X-rays with respect to the normal at the surface of the sample.

In the present study, the effective incident photon flux $I_0G\varepsilon_{K_i}$ ($i = \alpha$, β) for the Si(Li) detector in the range 34–96 keV has been evaluated using the equation [23]

$$I_0 G \varepsilon_{K_i} = \frac{N_{K_i}}{\beta_{K_i} m \sigma_{K_i}} \tag{3}$$

where N_{K_i}, β_{K_i} and m and have the same meaning as in equation (1) and σ_{K_i} represents the K X-ray fluorescence cross-sections. The absolute efficiency ε of the X-ray detector was determined by collecting the K X-ray spectra of samples of Ce, Nd, Gd, Dy, Er, Yb, Ta, Ir, Hg, Bi, Th, and U in the same experimental set-up.

The factor $I_0G\varepsilon_{K_i}$ was fitted as a function of energy using the equation

$$I_0 G \varepsilon_{K_{\mathrm{x}}} = A_0 + A_1 E_{\mathrm{x}} + A_2 E_{\mathrm{x}}^2 + A_3 E_{\mathrm{x}}^3 \tag{4}$$

$$= \sum_{i,n=0}^{3} A_i E_{\mathrm{x}}^n \tag{5}$$

where E_{x} is the K_α and K_β X-ray energy and A_0, A_1, A_2 and A_3 are constants evaluated from a fitting polynomial. The variation of the factor $I_0G\varepsilon_{K_i}$ as a function of the mean K X-ray energy is shown in Figure 2. The values of the factor $I_0G\varepsilon_{K_i}$ ($i = \alpha_1, \alpha_2, \beta_1, \beta_2$) for each K X-ray line of average energy E_{K_i} are interpolated from equation (4).

Table 1. Comparison of experimental and theoretical K X-ray production cross-sections.

Elements	$\sigma_{K_{\alpha 1}}$(b/atom)			$\sigma_{K_{\alpha 2}}$(b/atom)			$\sigma_{K_{\beta 1}}$(b/atom)			$\sigma_{K_{\beta 2}}$(b/atom)		
	Present Exp. Values	Theoretical predictions HF[15]	HS[16]	Present Exp. Values	Theoretical predictions HF[15]	HS[16]	Present Exp. Values	Theoretical predictions HF[15]	HS[16]	Present Exp. Values	Theoretical predictions HF[15]	HS[16]
^{58}Ce	99.57 ± 7.96	–	115.42	72.72 ± 5.80	–	63.01	28.41 ± 2.27	–	33.25	6.33 ± 0.50	–	8.07
^{59}Pr	117.93 ± 9.43	–	123.39	71.11 ± 5.68	–	67.60	28.98 ± 2.31	–	35.85	6.76 ± 0.54	–	8.74
^{60}Nd	119.71 ± 9.57	129.94	131.73	82.70 ± 6.61	71.35	72.31	37.11 ± 2.96	40.09	38.57	8.87 ± 0.71	10.28	9.45
^{62}Sm	147.86 ± 11.82	–	149.47	93.55 ± 7.48	–	82.65	47.20 ± 3.77	–	44.45	11.50 ± 0.92	–	10.95
^{63}Eu	142.66 ± 11.41	156.54	158.72	91.81 ± 7.34	86.73	87.93	47.08 ± 3.76	49.24	47.56	12.10 ± 0.96	12.70	11.75
^{64}Gd	165.76 ± 13.26	166.05	168.23	101.90 ± 8.15	92.29	93.53	55.22 ± 4.41	52.56	50.80	14.30 ± 1.14	13.79	12.75

HF: Hartree-Fock, HS: Hartree-Slater.

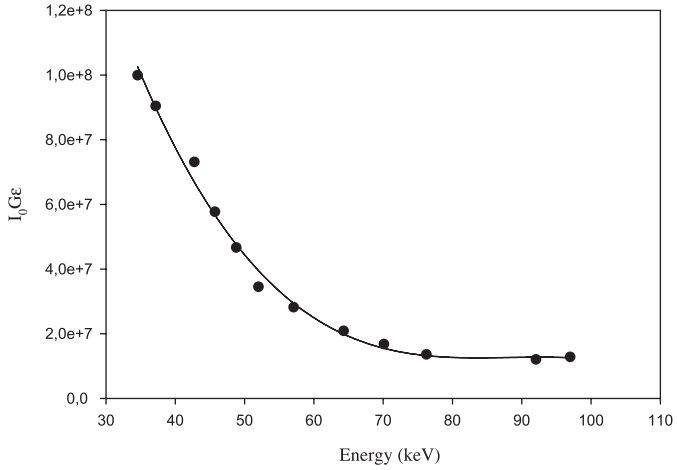

Fig. 2. The variation of the factor $I_0 G\varepsilon$ as a function of the mean K X-ray energy.

The K shell fluorescence yields were measured using the relation

$$\omega_K = \frac{\sigma_K^{\mathrm{x}}}{\sigma_K^P(E)} \tag{6}$$

where $\sigma_{K_i}^{\mathrm{x}}$ is the total K shell X-ray production cross-section and σ_K^P is the K shell photoionization cross-section for given element at excitation energy (E), taken from Scofield [27].

The $\mathrm{K}_\beta/\mathrm{K}_\alpha$ X-ray intensity ratio values have been calculated using the relation [28]

$$\frac{IK_\beta}{IK_\alpha} = \frac{N_{\mathrm{K}_\beta}}{N_{\mathrm{K}_\alpha}} \frac{\beta_{\mathrm{K}_\alpha}}{\beta_{\mathrm{K}_\beta}} \frac{\varepsilon_{\mathrm{K}_\alpha}}{\varepsilon_{\mathrm{K}_\beta}} \tag{7}$$

where N_{K_β} and N_{K_α} are the net counts under the K_β and K_α peaks, β_{K_β} and $\beta_{\mathrm{K}_\alpha}$ are the self-absorption correction factor of the target $\varepsilon_{\mathrm{K}_\beta}$ and $\varepsilon_{\mathrm{K}_\alpha}$ are the detector efficiency for K_β and K_α X-rays, respectively.

3.2 Theoretical evaluation

The theoretical K X-ray production cross-sections were evaluated by using the relation [17]

$$\sigma_{K_i}^{\mathrm{x}} = \sigma_K^P(E)\, \omega_K F_{K_i} \tag{8}$$

where $\sigma_K^P(E)$ and ω_K have the same meaning as in equation (6), F_{K_i} is the fractional X-ray emission rate for K_i X-rays and are defined as

$$F_{\mathrm{K}_{\alpha 1}} = \frac{I_{\mathrm{K}_{\alpha 1}}}{I_{\mathrm{K}_\alpha} + I_{\mathrm{K}_\beta}} \tag{9}$$

$$F_{\mathrm{K}_{\alpha 2}} = \frac{I_{\mathrm{K}_{\alpha 2}}}{I_{\mathrm{K}_{\alpha 1}}} F_{\mathrm{K}_{\alpha 1}} \tag{10}$$

$$F_{\mathrm{K}_{\beta_1'}} = \frac{I_{\mathrm{K}_{\beta_1'}}}{I_{\mathrm{K}_{\alpha 1}}} F_{\mathrm{K}_{\alpha 1}} \tag{11}$$

$$F_{\mathrm{K}_{\beta_2'}} = \frac{I_{\mathrm{K}_{\beta_2'}}}{I_{\mathrm{K}_{\alpha 1}}} F_{\mathrm{K}_{\alpha 1}} \tag{12}$$

where I_{K_i} is the K_i X-ray intensity. The values of intensity ratios were taken from Scofield based on relativistic Hartree-Fock theory [15] and relativistic Hartree-Slater theories [16]. The values of semi-empirical values ω_K were taken from the fitted values of Bambeynk et al. [29].

4 Result and discussion

The present measured and theoretical (based on relativistic Hartree-Fock and Hartree-Slater theories calculated by Scofield [15,16]) values of the K_i ($i = \alpha_1$, α_2, β_1 and β_2) X-ray production cross-sections in the atomic range $58 \leqslant Z \leqslant 64$ are listed in Table 1.

In earlier experiment [22], the authors used the same method for K X-ray production cross-sections, but they only measured K_i ($i = \alpha$ and β) X-ray production cross-sections ($\sigma_{\mathrm{K}_\alpha}$ and $\sigma_{\mathrm{K}_\beta}$) in the atomic region $40 \leqslant Z \leqslant 70$ at 122 keV photon. So this values can not been compared with the present values. The present values have been plotted as a function of the atomic number as shown in Figures 3a–3d. As can be seen from this figure, the K X-ray production cross-section values increase with increasing atomic number since three reasons: (i) increase in the fluorescence yield with Z; (ii) the possible increase in the K-shell photoionization cross-section at a given photon energy with Z because with increasing Z, the photon energy is closer and closer to the K-shell ionization threshold; (iii) outer shells have more electrons than smaller atomic number elements. It can be seen from Table 1 and Figures 3a–3d that the experimental values are in good

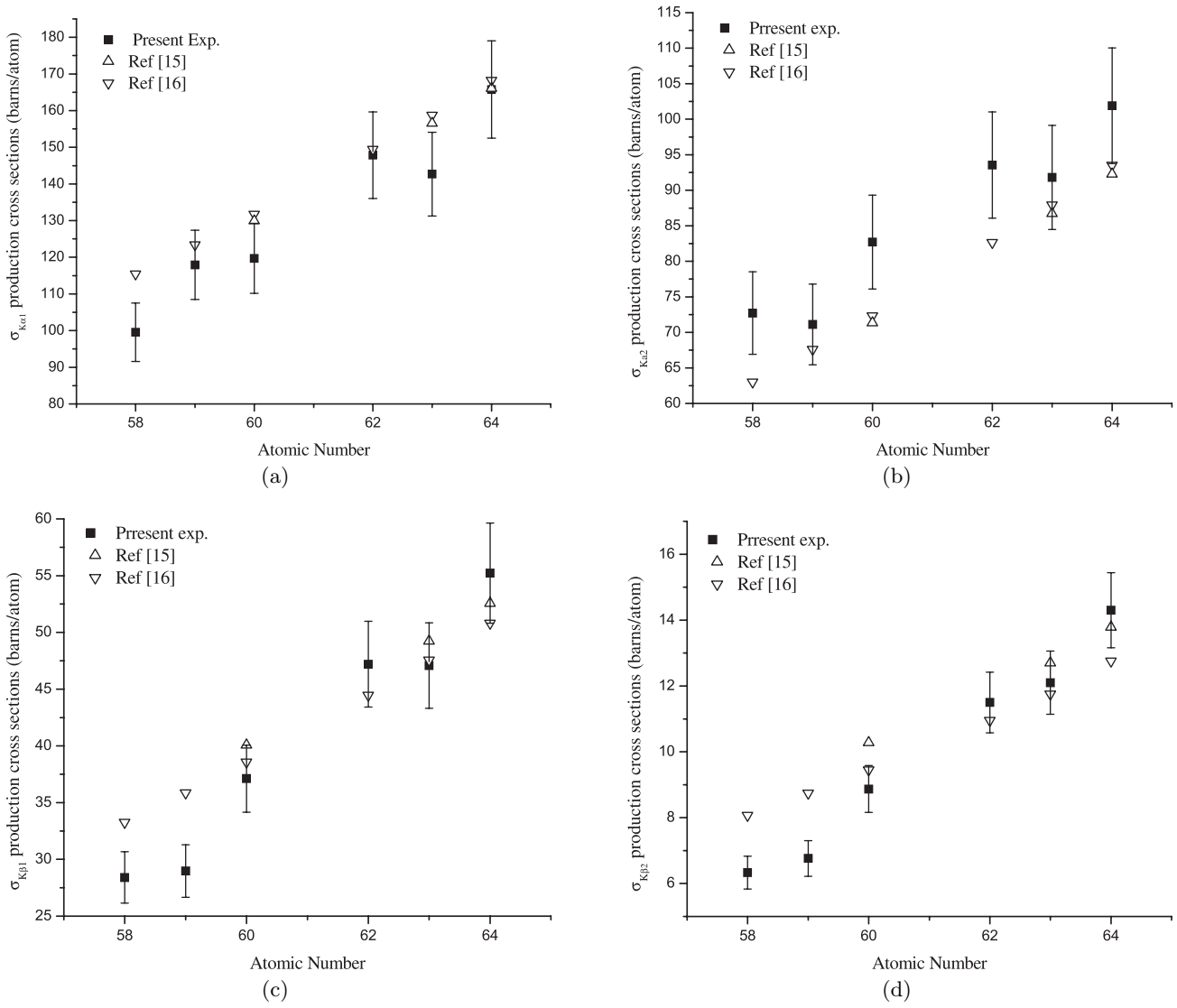

Fig. 3. Comparison of measured K shell X-ray production cross-sections, $\sigma^{x}_{K_i}$, with theoretical values as a function of atomic numbers (a–d).

agreement with the theoretical ones within the experimental uncertainties. Because experimental results for K_i ($i = \alpha_1$, α_2, β_1 and β_2) X-ray production cross-sections at the same energy cannot be found in the literature, the comparison is not made with the other experimental values. The agreement between the presently measured K X-ray production cross-sections and theoretical predictions for Sm, Eu and Gd are good within the range 0.2–9% for Hartree-Fock and 1–12% for Hartree-Slater theory, respectively. In addition, the same agreement for Ce Pr and Nd is changed within the range 8–13% and 4–25% for Hartree-Fock and Hartree-Slater theory, respectively. K_{β_2} and K_{β_1} cross-sections for these elements might caused this large values because of peak overlapping. One other reason for that may be the chemical effects.

The experimental error is estimated to be more than 8% and is getting larger with decreasing atomic number. It might be several reasons for this effect. The most important one is the very strongly dependence of detector efficiency with decreasing energy. This error is attributed to the uncertainties in different parameters used to deduce K X-ray production cross-section, K X-ray fluorescence yields and K_β/K_α values; namely, the error in the area evaluation under the K_α and K_β X-ray peak ($\leqslant$3%), in the absorption correction factor ratio ($\leqslant$2%), the product $I_0 G\varepsilon$ (5–7%) and the other systematic errors (2–3%). In this work, in order to reduce the absorption, thin samples were used as the target; furthermore, an absorption correction was also performed for each sample. In order to reduce the statistical error, the spectra were recorded and about 10^3–10^6 (or more) counts were collected under the K_α and K_β peaks. Fitting the measured spectra with multi-Gaussian functions plus polynomial backgrounds using software program separated the K_α and K_β photopeak areas.

Table 2. K shell fluorescence yields ω_K.

Elements	ω_K		
	Present Exp.	Semi-empirical Theoretical predictions	
	Values	reference [8]	reference [29]
^{58}Ce	0.857 ± 0.068	0.912	0.910
^{59}Pr	0.872 ± 0.069	0.917	0.914
^{60}Nd	0.904 ± 0.072	0.921	0.918
^{62}Sm	0.967 ± 0.077	0.929	0.926
^{63}Eu	0.891 ± 0.071	0.932	0.929
^{64}Gd	0.966 ± 0.077	0.935	0.932

Table 3. K shell intensity ratios K_β/K_α.

Elements	K_β/K_α		
	Present Exp. Values	Theoretical predictions	
		HF [15]	HS [16]
^{58}Ce	0.2460 ± 0.005	–	0.2316
^{59}Pr	0.2376 ± 0.005	–	0.2336
^{60}Nd	0.2402 ± 0.005	0.2504	0.2354
^{62}Sm	0.2451 ± 0.008	–	0.2389
^{63}Eu	0.2549 ± 0.003	0.2549	0.2405
^{64}Gd	0.2622 ± 0.005	0.2570	0.2426

HF: Hartree-Fock, HS: Hartree-Slater.

The K X-ray fluorescence yields ω_K derived from the experimental data have been compared with the values tabulated by Krause [8] and Bambeynk et al. [29]. As can be seen in Table 2 that our experimental values closely agree with them. Furthermore, the experimental K X-ray K_β/K_α intensity ratios are also in agreement with the theoretical values calculated for these elements (see Tab. 3). We believe that the obtained data will be helpful to those using radioisotope XRF techniques for elemental analysis.

References

1. S. Oizane, A. Amokrane, M. Zilabdi, Nucl. Instrum. Meth. B **161–163**, 141 (2000)
2. D.V. Rao, R. Cesareo, G.E. Gigante, X-ray Spectrom. **22**, 406 (1993)
3. L.A. Al-Nasr, I.J. Jabr, K.A. Al-Saleh, N.S. Saleh, Appl. Phys. A. **43**, 71 (1987)
4. N.S. Saleh, K.A. Al-Saleh, Appl. Radiat. Isot. **11**, 975 (1987)
5. M. Ertugrul, Anal. Chim. Acta. **491**, 239 (2003)
6. M.O. Krause, C.V. Nester, J. Sparks, E. Ricci, Oak Ridge National Laboratory, 5399 Report (ORNL) (1978)
7. W. Bambynek, B. Crasemann, R.W. Fink, H.U. Freund, H. Mark, C.D. Swift, R.E. Price, P.V. Rao, Rev. Mod. Phys. **44**, 716 (1972)
8. M.O. Krause, J. Phys. Chem. Ref. Data. **8**, 307 (1979)
9. J.H. Hubbell, P.N. Trehan, N. Singh, B. Chand, D. Mehta, M.L. Garg, R.R. Garg, S. Singh, S. Puri, J. Phys. Chem. Ref. Data. **23**, 339 (1994)
10. M. Ertuğrul, Ö Söğüt, Ö Şimşek, E. Büyükkasap, J. Phys. B: At. Mol. Opt. Phys. **34**, 909 (2001)
11. B.B. Dhal, H.C. Padhi, Phys. Rev. A. **50**, 1096 (1994)
12. M. Ertuğrul, Ö. Şimşek, J. Phys. B: At. Mol. Opt. Phys. **35**, 601 (2002)
13. V.N. Rao, S.B. Reddy, G. Satyanarayana, D.L. Sastry, Physica B **143** 375 (1986)
14. U. Çevik, İ. Değirmencioglu, B. Ertuğral, G. Apaydin, H. Baltaş, Eur. Phys. J. D **23**, 29 (2005)
15. J.H. Scofield, Phys. Rev. A **9**, 1041 (1974)
16. J.H. Scofield, At. Data Nucl. Data Tables **14**, 121 (1974)
17. N.S. Saleh, A.J. Abu El-Haija, J. Phys. B **21**, 3077 (1988)
18. S. Seven, Turk. J. Phys. **26**, 483 (2002)
19. G. Apaydın, E. Tırasoğlu, Nucl. Instrum. Meth. B **246**, 303 (2006)
20. A.S. Bennal, P.D. Shidling, N.M. Badiger, S.R. Thontadarya, B. Hanumaiah, Am. J. Phys. **73**, 883 (2005)
21. Y. Özdemir, R. Durak, E. Öz, Rad. Phy. And Chem. **65**, 199 (2002)
22. R. Durak, S. Erzenoglu, Y. Kurucu, Y. Şahin, Radiat. Phys. Chem. **51**, 45 (1998)
23. B. Ertuğral, G. Apaydın, H. Baltaş, U. Çevik, A.İ. Kobya, M. Ertuğrul, Spect. Acta B **60**, 519 (2005)
24. G. Apaydın, E. Tıraşoğlu, U. Çevik, B. Ertuğral, H. Baltaş, M. Ertuğrul, A.İ. Kobya, Radiat. Phys. Chem. **72**, 549 (2005)
25. M.J. Berger, J.H. Hubbell, XCOM: NBSIR85-3597, National Bureau of Standards, Gaithersburg, MD, USA, for version 3.1 (1999) see `http://physics.nist.gov/`
26. E. Storm, I. Israel, Nucl. Data. Tables A **7**, 565 (1970)
27. J.H. Scofield, Lawrence Livermore Laboratory (UCRL) **51326**, (1973)
28. B. Ertuğral, G. Apaydın, A. Tekbıyık, E. Tirasoğlu, U. Çevik, A.İ. Kobya, M. Ertuğrul, Eur. Phys. J. D **37**, 371 (2006)
29. W. Bambeynk, *Molecules and Solids A*, Meisel, Leipzig DDR (1984) Paper P I